Dehydration-Driven Ion Aggregation and the Onset of Gelation in $ZnCl_2$ Solution

Alexei V. Tkachenko,[1,*] Chuntian Cao,[2] Amy C. Marschilok,[3,4,5,6] and Deyu Lu[1,†]

[1]*Center for Functional Nanomaterials, Brookhaven National Laboratory, Upton, New York 11973, USA*
[2]*Artificial Intelligence Department, Brookhaven National Laboratory, Upton, New York 11973, USA*
[3]*Interdisciplinary Science Department, Brookhaven National Laboratory, Upton, New York 11973, USA*
[4]*Institute of Sustainability, Electrification and Energy (I:SEE), Stony Brook University, Stony Brook, New York 11794, USA*
[5]*Department of Chemistry, Stony Brook University, Stony Brook, New York 11794, USA*
[6]*Department of Materials Science and Chemical Engineering, Stony Brook University, Stony Brook, New York 11794, USA*

(Received 19 December 2025; accepted 24 July 2026; published 18 August 2026)

A minimal model of ionic aggregation in concentrated $ZnCl_2$ is developed, guided by molecular dynamics simulations with a machine-learned potential. It explicitly incorporates solvent-site depletion, correlated chloride binding, and allows for loops within Zn–Cl clusters. Dehydration drives two coordination-controlled structural changes: a crossover at $Z = 2$ from predominantly isolated Zn-containing species to Cl-bridged clusters and the onset of gelation near $Z \approx 3$. The model reproduces the concentration-dependent trends observed in the molecular dynamics simulations with two fitted parameters, while the cluster-size distribution at the highest concentration is consistent with three-dimensional percolation scaling over the accessible range of cluster sizes.

DOI: 10.1103/gxkq-6zw4

I. INTRODUCTION

Highly concentrated "water-in-salt" (WIS) electrolytes exhibit a physicochemical behavior that lies well outside the scope of classical dilute-ion descriptions. Among them, $ZnCl_2$ stands out as one of the most soluble inorganic salts containing a multivalent cation [1]. Its exceptional solubility and anomalous properties are widely attributed to the formation of stable multi-ion complexes such as $ZnCl_4^{2-}$. These complexes also enable highly concentrated $ZnCl_2$ solutions to dissolve cellulose, a property exploited since the 19th century [1]. Beyond its importance as a model WIS system, $ZnCl_2$ is technologically relevant for next-generation zinc-ion batteries, which were found to suppress the water-splitting reactions, help regulate the morphologies of Zn plating, and improve the Coulombic efficiency of Zn anodes [2].

Recent atomic simulations [3] suggest that Zn ion aggregates can form in the WIS regime with a strong impact on ion transport, yet the microscopic structure and connectivity of multi-ion aggregates in the WIS regime remain poorly understood. This behavior is qualitatively consistent with earlier theoretical models [4–6] that draw analogies between ionic aggregation and classical Flory-Stockmayer (FS) [7–9] theories to describe superconcentrated ionic solutions. In those models, ions and solvent molecules are represented as patchy particles characterized by a maximum number of bonds ("patches"), and bond formation is taken to be independent among patches and determined solely by the availability of unbound sites, producing loopless Cayley-tree clusters with fixed degree distributions.

In the present paper, we combine molecular dynamics (MD) simulations based on a machine-learning interatomic potential (MLIP) [3] with an analytic model to uncover the mechanism behind ionic aggregation in $ZnCl_2$ WIS electrolytes. Our minimal model is conceptually related to the FS-based picture [4–9] but incorporates several essential revisions motivated directly by our MD results. *First*, we lift the Cayley-tree constraint and allow loop formation, thereby going beyond the loopless FS description and motivating a comparison of the simulated cluster statistics with finite-dimensional percolation. *Second*, we relax the assumption of independent bond formation, specifically for chloride ligands, in order to capture the substantial free-energy penalty associated with forming a Cl-mediated Zn–Cl–Zn bridge. This correlated binding produces qualitatively distinct behavior, including

*Contact author: oleksiyt@bnl.gov
†Contact author: dlu@bnl.gov

the sharp coordination-driven crossover that we identify as the *aggregation threshold*. *Third*, guided by the known structure of Zn^{2+} and Cl^- hydration shells and supported by MD, we allow the effective topological valence of each species to differ between ion-ion and ion-water interactions. *Finally*, we treat the availability of hydrogen and oxygen sites of the water molecules as independent degrees of freedom, consistent with classical FS theory, but differently from the generic model of McEldrew *et al.* [4].

We show that progressive dehydration drives ion association, producing two distinct structural changes. The first, at an average Zn coordination number $Z = 2$, marks a sharp crossover from simple Zn–Cl association to the formation of branched Zn–Cl clusters in which chlorides bridge multiple Zn^{2+} ions. The second is the onset of gelation near $Z \approx 3$. At the highest simulated concentration, the broad cluster-size distribution is consistent with proximity to a three-dimensional percolation threshold, although the available system sizes and concentrations do not permit a determination of the universality class.

II. MD-MLIP SIMULATIONS

The MD trajectories were generated in our previous work [3] using a machine-learning interatomic potential trained with DeePMD-kit [10] on the density-functional-theory data using the SCAN functional [11–13] selected through the DP-GEN active-learning workflow [14]. Simulations were performed in LAMMPS [15] for six concentrations in periodic boxes containing 1600–2000 atoms. For each composition, three 100-ns trajectories were collected in the NpT ensemble at 333 K and 1 bar after 2 ns of equilibration, using a 0.5-fs time step. At 333 K, our SCAN MLIP reproduces the structure of ambient water in the literature [16,17]. The calculated structure factors of the $ZnCl_2$ solution agree well with available x-ray-scattering data [3]; additional training and simulation details are given in Supplemental Material [18].

The six aqueous $ZnCl_2$ compositions range from 1.05 m ($Zn:O = 1:53$) to 30 m ($Zn:O = 1:1.85$). Simulation snapshots at representative concentrations are shown in Fig. 1. The trajectories reveal that the first solvation shell of Zn^{2+} comprises both H_2O and Cl^- ligands, with coordination numbers varying from 4 to 6. Fully hydrated $Zn(H_2O)_6^{2+}$ is octahedral, while $ZnCl_4^{2-}$ is tetrahedral. Intermediate complexes $Zn(H_2O)_xCl_y$, $x + y = 4$–6, form distorted polyhedra whose chloride content increases with concentration, reflecting progressive ligand substitution. Because each Cl^- can bridge two Zn^{2+} centers, partially chlorinated solvation shells interconnect via shared chlorides, forming extended Zn–Cl aggregates [1,19]. In the WIS regime, these aggregates merge into polymer-like ion networks spanning nanometer scales. This evolution from discrete complexes to extended networks provides a structural basis for the concentration dependence of ion transport and for the onset of gelation.

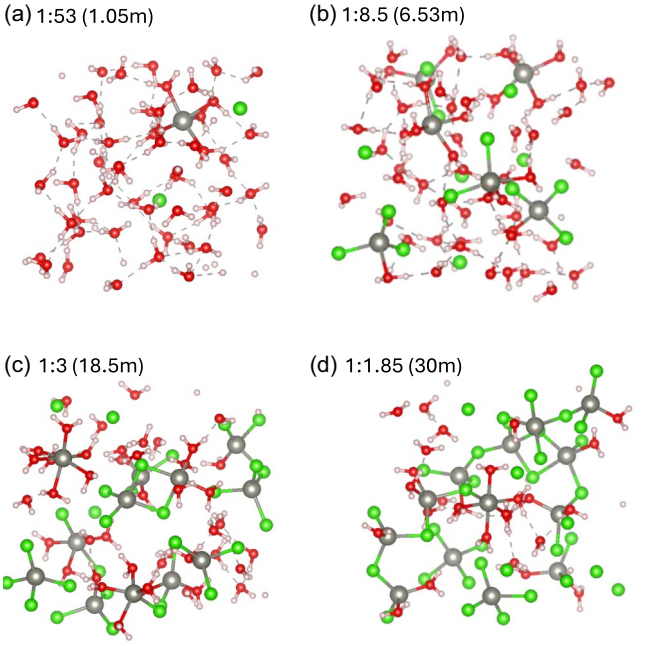

FIG. 1. MD simulation snapshots taken at different salt concentrations. (a) salt-to-water molecular ratio $n_s = 1:53$ (molality 1.05 m); (b) $n_s = 1:8.5$ (6.53 m); (c) $n_s = 1:3$ (18.5 m); (d) $n_s = 1:1.85$ (30 m).

III. MINIMAL MODEL

A. Bridging equilibrium

In our model (presented in full detail in Supplemental Material [18]), each Zn^{2+} provides four equivalent coordination sites for Cl^-. Chlorides may be terminal (bound to one Zn) or bridging (shared by two). The central variables are the free-chloride fraction α, defined as the fraction of all chloride ions that are not coordinated to Zn^{2+}, the mean Zn–Cl coordination number Z, the bridging fraction p, and the salt-to-water molecular ratio $n_s = C_s/C_w$, where C_s and C_w represent salt and water concentrations, respectively. Terminal Cl^- contributes one Zn–Cl bond, while a bridge contributes two, giving the coordination balance

$$Z = 2(1-\alpha)(1+p). \tag{1}$$

The conversion of two terminals into a bridge releases one free chloride, as shown in Fig. 2(a), yielding the equilibrium condition:

$$\frac{p}{K(1-p)^2} = \frac{1-\alpha}{\alpha}, \tag{2}$$

where the dimensionless constant $K \ll 1$ encodes the electrostatic and entropic penalties of bridging.

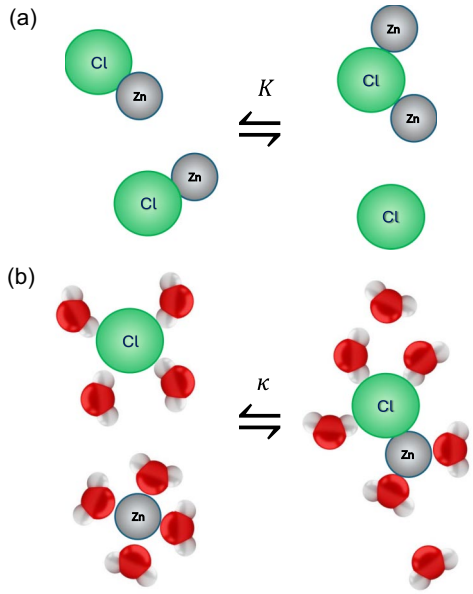

FIG. 2. Schematic representation of the key processes in the model. (a) Bridging reaction. (b) Hydration-dependent association of Zn^{2+} and Cl^- ions.

Combining Eqs. (1) and (2) gives

$$\alpha(p) = \frac{1}{1 + p/[K(1-p)^2]}, \tag{3}$$

$$Z(p) = \frac{2(1+p)}{1 + K(1-p)^2/p}. \tag{4}$$

As shown in Fig. 3, these relations reproduce the observed evolution of α and p with Z across the simulated concentration range.

Two regimes emerge with a sharp crossover at $Z = 2$. For $Z < 2$, $\alpha \approx 1 - Z/2$, and $p \approx 0$, corresponding to dissociated ions and small clusters. For $Z > 2$, $\alpha \approx 0$, and $p \approx Z/2 - 1$, signaling extensive aggregation. This reflects the large free-energy cost of Zn–Cl–Zn bridging: at low Z, the system favors isolated ions and single-Zn clusters; but once $Z = 2$, chloride scarcity forces the system to use bridges, driving rapid aggregation. We therefore identify $Z = 2$ as the *aggregation threshold*. This crossover and the comparison in Fig. 3 are robust when K is sufficiently small. Changing K from 3×10^{-4} to 10^{-6} primarily narrows the crossover region near $Z = 2$ while leaving the predicted trends outside that region nearly unchanged. Both curves provide a comparable description of the MD data; the comparison is intended to demonstrate robustness rather than a precise determination of K.

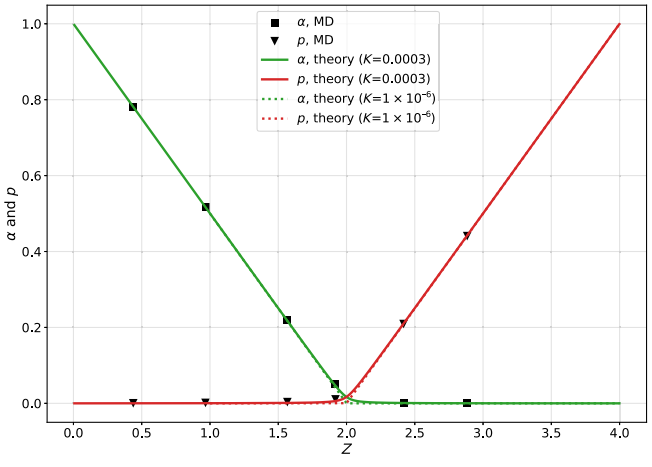

FIG. 3. Theoretical relationships between $p(Z)$ and $\alpha(Z)$ compared with MD data (symbols) for $K = 3 \times 10^{-4}$ (solid) and $K = 10^{-6}$ (dotted).

B. Dehydration-driven ion aggregation

The preceding argument explains why a sharp crossover occurs at $Z = 2$, but it does not by itself guarantee that the solution can reach this point prior to becoming saturated. To illustrate the limitation, first consider a naive model in which binding between free chloride and vacant Zn sites is described by a single association constant $\tilde{K}$:

$$\tilde{K}[\mathrm{Cl}^-][\mathrm{Zn-site}] = [\mathrm{Cl_t}], \tag{5}$$

$$\tilde{K}\, C_s(4 - Z) = \frac{1-\alpha}{\alpha}. \tag{6}$$

Here all bracketed quantities are number concentrations and $\tilde{K}$ has units of inverse concentration. In this naive, nonbridging limit, $[\mathrm{Cl}^-] = 2\alpha C_s$, $[\mathrm{Zn-site}] = (4 - Z)C_s$, and $[\mathrm{Cl_t}] = 2(1-\alpha)C_s$; substitution into the first equation cancels the common factor $2C_s$ and yields the second equation. Thus, no concentration factor is implicitly absorbed into $\tilde{K}$. The free-chloride fraction α then decreases only as $1/C_s$. At $Z = 2$, Eqs. (1) and (2) give $\alpha \simeq \sqrt{K}$ for $K \ll 1$. Reaching this value in the naive model would require $C_s \sim 1/(\tilde{K}\sqrt{K})$, up to a numerical factor of order unity. The required concentration is therefore larger than the initial association scale $1/\tilde{K}$ by a factor of order $1/\sqrt{K}$, giving an unrealistic estimate above 10^2 m for the parameters relevant here.

The naive association model does not take into account that at high enough salt concentration the availability of water molecules for the hydration of free ions becomes a limiting factor. To capture the separate scarcity of hydrogen donors (for anion hydration) and oxygen acceptors (for cation hydration), we introduce two dimensionless coefficients, γ_{H} and γ_{O}, the solvent-site activity coefficients for hydrogen and oxygen sites, respectively. They play the role of activity coefficients for the respective solvent sites: $\gamma = 1$ indicates ideal availability; $\gamma < 1$ indicates scarcity.

We begin with O sites. A fully hydrated Zn^{2+} ion has $s_0 = 6$ oxygen ligands in the first shell, while a tetrahedral $ZnCl_4$ species has none. Thus, each Zn–Cl bond, on average, blocks $s \approx 3/2$ oxygen-binding sites. If $(1-\gamma_O)C_w$ denotes the population of O sites that are effectively sequestered, a mass-action balance leads to

$$K_O \gamma_O C_w\big((s_0 - sZ)C_s - (1-\gamma_O)C_w\big) = (1-\gamma_O)C_w. \tag{7}$$

Here the association constant K_O characterizes the affinity of an O site of a water molecule for a Zn^{2+} ion. A similar relation can be written for γ_H, assuming that hydration of a free Cl^- requires h_0 H-donor sites and that each Zn–Cl bond frees h of them. Because the Cl^- hydration shell is less structured than that of Zn^{2+}, we take $h_0 = 8$ and treat h as a fitting parameter. From the above balance equation, one obtains

$$\gamma_O - \frac{\epsilon_O}{\gamma_O} \approx 1 + n_s(sZ - s_0), \tag{8}$$

$$\gamma_H - \frac{\epsilon_H}{\gamma_H} \approx 1 + n_s\left(\frac{hZ}{2} - h_0\right), \tag{9}$$

with $\epsilon_O = 1/(K_O C_w) \ll 1$ and $\epsilon_H = 1/(2K_H C_w) \ll 1$.

Associating a Cl^- with a vacant Zn site releases s oxygen sites and h hydrogen sites, as schematically shown in Fig. 2(b):

$$\mathrm{Zn-site} + Cl^- \rightleftharpoons \mathrm{Zn-Cl} + s\,O + h\,H. \tag{10}$$

Mass-action equilibrium gives

$$\frac{1-\alpha}{\alpha} = \frac{\kappa n_s}{\gamma_O^s \gamma_H^h}\,\frac{4-Z}{1-p}, \tag{11}$$

where $\kappa = 2^{-h}K_a C_w^{1-(s+h)}$ is the dimensionless reduced association constant; the factor 2^{-h} follows from the two H-donor sites per water molecule. Combining Eqs. (11), (2), and (4) yields the full dependence of Z, p, and α on n_s. Figure 4 compares the theoretical predictions.

Only two parameters, κ and h, are adjusted in the comparison with the MD data. The remaining parameters are fixed by hydration-shell structure ($s_0 = 6$, $s = 3/2$, and $h_0 = 8$) or have weak effects in the relevant regime. Changing K from 3×10^{-4} to 10^{-6} mainly sharpens the crossover near $Z = 2$, while varying ϵ_O and ϵ_H has little effect when both are $\lesssim 0.01$. The curves in Fig. 4 use $\kappa = 4$ and $h = 4.45$ for $K = 10^{-6}$ or $h = 5.15$ for $K = 3 \times 10^{-4}$. With the two fitted parameters, the model simultaneously captures the concentration trends of Z, p, and α. In Supplemental Material [18], we provide a detailed discussion of the model parameters, including their physical estimates and sensitivity tests. In particular, the best-fit value of κ is shown to be consistent with known stepwise

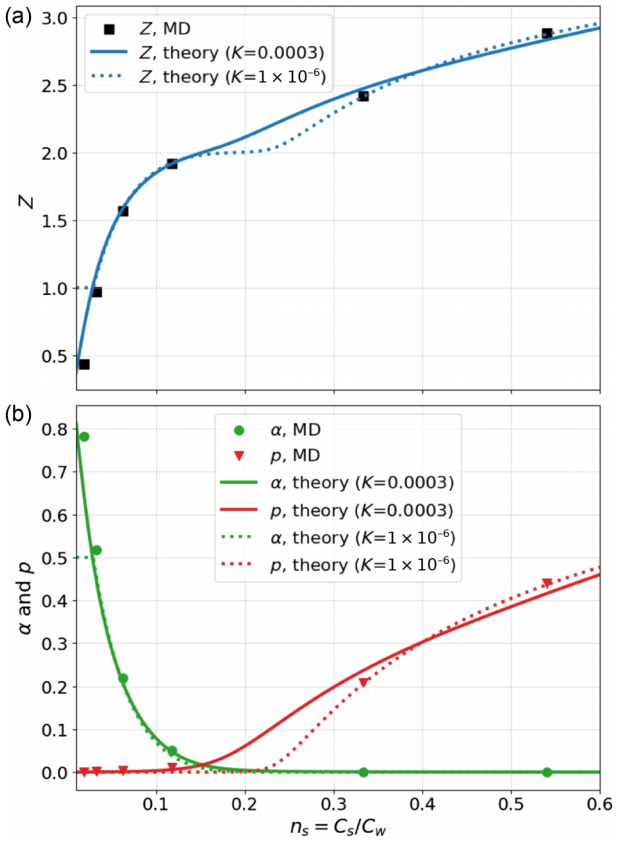

FIG. 4. Comparison of the theoretical mean Zn–Cl coordination number Z [panel (a)], bridging probability p, and free-chloride fraction α with MD simulations [panel (b)].

association constants for $ZnCl_n$ complexes after accounting, at a semiquantitative level, for the suppression of ion association at high ionic strength [20–22].

C. Gelation criticality

Our system belongs to the broad class of gelation and percolation models for branched-monomer networks. Classical FS theory predicts gelation for monomers of functionality f when the bond-formation probability exceeds $p_b > p_c = 1/(f-1)$. For $ZnCl_2$, the relevant functionality is $f = 4$, and the effective Zn–Zn bonding probability is $Zp/4$, which yields the gelation condition

$$Z(Z-2) > 8p_c, \tag{12}$$

$$Z_c = 1 + \sqrt{1 + 8p_c}\,. \tag{13}$$

Using the FS value $p_c = 1/3$ gives $Z_c \approx 2.91$ [7,8]. Because FS theory neglects loops, its threshold and cluster statistics provide a mean-field reference rather than a complete description of the simulated network [23]. For comparison, bond percolation on the diamond lattice, which also has functionality $f = 4$, has $p_c \approx 0.39$ and yields $Z_c \approx 3.03$ [24]. At the highest concentration studied

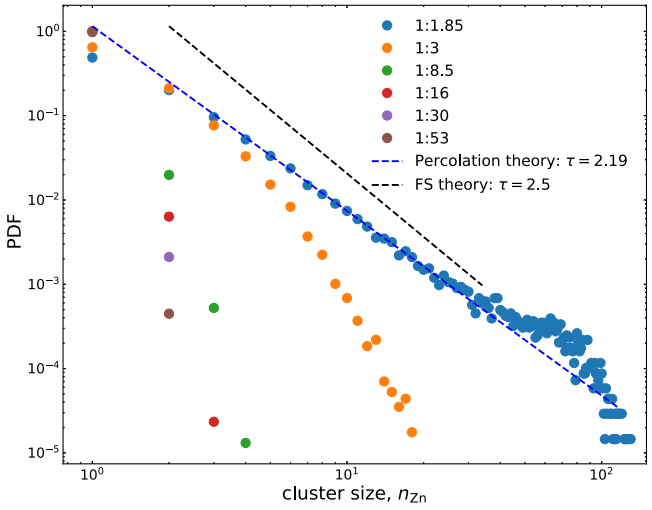

FIG. 5. Cluster-size distributions from MD simulations for Zn–Cl aggregates at different concentrations, plotted on logarithmic axes. The markers show the probability density as a function of the number n_{Zn} of Zn^{2+} ions per cluster. For the 30-m electrolyte (Zn:O = 1:1.85), the distribution is broad and is consistent, over the accessible intermediate-size range, with the three-dimensional percolation reference $f \sim n_{Zn}^{-2.19}$. The loopless FS reference, $f \sim n_{Zn}^{-5/2}$, is shown for comparison. The finite simulation size and limited concentration sampling preclude an independent determination of the exponent. PDF is defined as probability density function.

($n_s = 1$: 1.85 or 30 m), the mean coordination number approaches this value. We therefore examine whether the corresponding cluster-size distribution is consistent with proximity to a percolation threshold.

Near a percolation transition, the cluster-size distribution is expected to exhibit an approximate power-law regime, $f(n) \sim n^{-\tau}$ [23]. Loopless FS theory gives $\tau_{FS} = 5/2$ [7,8], whereas three-dimensional percolation has $\tau \approx 2.19$ [23,24]. Figure 5 shows the cluster-size distributions obtained from the MD simulations. At the highest concentration, the distribution is broad, extending from isolated Zn^{2+} ions to aggregates containing approximately 130 Zn^{2+} ions. Over the accessible intermediate-size range, the data are visually consistent with a power law close to $\tau = 2.19$ and are less steep than the FS reference $\tau = 5/2$. Because the simulations include a single finite system at each of six concentrations, with no finite-size scaling or independent exponent uncertainty, this comparison should be interpreted as evidence consistent with three-dimensional percolation-like behavior, not as a determination of a universality class.

IV. DISCUSSION

The two coordination scales identified here describe different physical phenomena. The crossover at $Z = 2$ follows from chloride bookkeeping in the presence of a strong penalty for Zn–Cl–Zn bridge formation: once terminal coordination consumes nearly all available chloride, further growth of Z requires shared ligands and therefore produces rapid cluster growth. Gelation near $Z \approx 3$, in contrast, is a collective connectivity condition whose location depends on the effective bonding probability and loop formation. It should therefore not be interpreted as a second local chemical-equilibrium transition.

The model also provides a structural interpretation of the concentration-dependent transport behavior reported for the same simulated electrolytes [3]. Dehydration reduces the population of free chloride ions while increasing the size and connectivity of Zn-containing aggregates. For aqueous Zn batteries, this highlights a trade-off: reduced water activity can suppress water-driven side reactions and modify Zn deposition, while the accompanying ion association can reduce the mobility of independent charge carriers [2,3]. The present equilibrium model does not calculate transport coefficients or interfacial kinetics, but the variables Z, p, and α provide compact structural descriptors for connecting electrolyte composition to charge-carrier speciation.

In summary, our combined molecular dynamics simulations and analytic modeling demonstrate that progressive dehydration is the key microscopic driver of ion aggregation and gelation in concentrated $ZnCl_2$ solutions. As water becomes scarce, chloride ligands increasingly bridge neighboring Zn^{2+} centers, leading to a hierarchy of structural changes. The first occurs at an average coordination number $Z = 2$, marking the crossover from isolated ionic complexes $ZnCl_x$ to branched clusters containing multiple Zn^{2+} ions. The second, near $Z \approx 3$, is associated with the onset of a connected Zn–Cl network analogous to the sol-gel transition in branched polymer systems. The broad cluster-size distribution at the highest simulated concentration is consistent with near-critical three-dimensional percolation behavior but does not by itself establish a universality class.

These findings establish a direct connection between local coordination chemistry and emergent mesoscale connectivity in aqueous $ZnCl_2$. They identify dehydration-induced chloride bridging as the mechanism responsible for the structural evolution observed in this system. Similar competition between ion hydration and bridging may operate in other highly concentrated electrolytes, but establishing the range of applicability of this mechanism will require tests in additional chemical systems.

ACKNOWLEDGMENTS

This research has been conducted and used resources of the Theory and Computational Facility of the Center for Functional Nanomaterials, which is a U.S. Department of Energy Office of Science User Facility, at Brookhaven National Laboratory under Contract No. DE-SC0012704. This research was partially funded by the U.S. Department

of Energy, Office of Science, Basic Energy Sciences, through Contract No. DE-SC0012704, under the Materials Chemistry program.

DATA AVAILABILITY

The data supporting the findings of this study are available from the corresponding author upon reasonable request.

[1] X. Ji, *A perspective of* $ZnCl_2$ *electrolytes: The physical and electrochemical properties*, eScience **1**, 99 (2021).

[2] F. Wang, O. Borodin, T. Gao, X. Fan, W. Sun, F. Han, A. Faraone, J. A. Dura, K. Xu, and C. Wang, *Highly reversible zinc metal anode for aqueous batteries*, Nat. Mater. **17**, 543 (2018).

[3] C. Cao, A. Kingan, R. C. Hill, J. Kuang, L. Wang, C. Zhang, M. R. Carbone, H. van Dam, S. Yoo, S. Yan, E. S. Takeuchi, K. J. Takeuchi, X. Wu, A. M. M. Abeykoon, A. C. Marschilok, and D. Lu, *Resolving the solvation structure and transport properties of aqueous zinc electrolytes from salt-in-water to water-in-salt using neural network potential*, PRX Energy **4**, 023004 (2025).

[4] M. McEldrew, Z. A. H. Goodwin, S. Bi, M. Z. Bazant, and A. A. Kornyshev, *Theory of ion aggregation and gelation in super-concentrated electrolytes*, J. Chem. Phys. **152**, 234506 (2020).

[5] M. McEldrew, Z. A. H. Goodwin, S. Bi, A. A. Kornyshev, and M. Z. Bazant, *Ion clusters and networks in water-in-salt electrolytes*, J. Electrochem. Soc. **168**, 050514 (2021).

[6] Z. A. H. Goodwin, M. McEldrew, B. Kozinsky, and M. Z. Bazant, *Theory of cation solvation and ionic association in nonaqueous solvent mixtures*, PRX Energy **2**, 013007 (2023).

[7] P. J. Flory, *Molecular size distribution in three dimensional polymers. I. Gelation*, J. Am. Chem. Soc. **63**, 3083 (1941).

[8] W. H. Stockmayer, *Theory of molecular size distribution and gel formation in branched polymers II. General cross linking*, J. Chem. Phys. **12**, 125 (1944).

[9] F. Tanaka and W. H. Stockmayer, *Thermoreversible gelation with junctions of variable multiplicity*, Macromol. Symp. **81**, 171 (1994).

[10] H. Wang, L. Zhang, J. Han, and W. E, *DeePMD-kit: A deep learning package for many-body potential energy representation and molecular dynamics*, Comput. Phys. Commun. **228**, 178 (2018).

[11] P. Giannozzi *et al.*, *Quantum espresso: A modular and open-source software project for quantum simulations of materials*, J. Phys. Condens. Matter **21**, 395502 (2009).

[12] P. Giannozzi *et al.*, *Advanced capabilities for materials modelling with quantum espresso*, J. Phys. Condens. Matter **29**, 465901 (2017).

[13] J. Sun, A. Ruzsinszky, and J. P. Perdew, *Strongly constrained and appropriately normed semilocal density functional*, Phys. Rev. Lett. **115**, 036402 (2015).

[14] Y. Zhang, H. Wang, W. Chen, J. Zeng, L. Zhang, H. Wang, and W. E, *DP-GEN: A concurrent learning platform for the generation of reliable deep learning based potential energy models*, Comput. Phys. Commun. **253**, 107206 (2020).

[15] A. P. Thompson, H. M. Aktulga, R. Berger, D. S. Bolintineanu, W. M. Brown, P. S. Crozier, P. J. in 't Veld, A. Kohlmeyer, S. G. Moore, T. D. Nguyen, R. Shan, M. J. Stevens, J. Tranchida, C. Trott, and S. J. Plimpton, *LAMMPS—A flexible simulation tool for particle-based materials modeling at the atomic, meso, and continuum scales*, Comput. Phys. Commun. **271**, 108171 (2022).

[16] M. Chen, H.-Y. Ko, R. C. Remsing, M. F. C. Andrade, B. Santra, Z. Sun, A. Selloni, R. Car, M. L. Klein, J. P. Perdew, and X. Wu, *Ab initio theory and modeling of water*, Proc. Natl. Acad. Sci. U.S.A. **114**, 10846 (2017).

[17] J. A. Morrone and R. Car, *Nuclear quantum effects in water*, Phys. Rev. Lett. **101**, 017801 (2008).

[18] See Supplemental Material at http://link.aps.org/supplemental/10.1103/gxkq-6zw4 for additional details of MD simulations, a detailed derivation of the model, discussion of parameter estimates, and sensitivity tests.

[19] J.-H. Choi, H. R. Choi, J. Jeon, and M. Cho, *Ion aggregation in high salt solutions. VII. The effect of cations on the structures of ion aggregates and water hydrogen-bonding network*, J. Chem. Phys. **147**, 154107 (2017).

[20] P. Atkins and J. de Paula, *Atkins' Physical Chemistry*, 8th ed. (Oxford University Press, New York, 2009).

[21] A. E. Martell, R. M. Smith, and R. J. Motekaitis, *Critical Stability Constants* (Springer, New York, 2004), Vol. 6.

[22] P. Debye and E. Hückel, *The theory of electrolytes. I. Lowering of freezing point and related phenomena*, Phys. Z. **24**, 185 (1923).

[23] D. Stauffer and A. Aharony, *Introduction to Percolation Theory* (Taylor & Francis, London, 2018).

[24] X. Xu, J. Wang, J.-P. Lv, and Y. Deng, *Simultaneous analysis of three-dimensional percolation models*, Front. Phys. **9**, 113 (2013).